Effects of topology and size on statics and dynamics of complexes of hyperbranched polymers with linear polyelectrolytes

G. K. Dalakoglou and K. Karatasos[a)]
Physical Chemistry Laboratory, Chemical Engineering Department, Aristotle University of Thessaloniki, 54124 Thessaloniki, Greece

S. V. Lyulin
Institute of Macromolecular Compounds, Russian Academy of Sciences, Bolshoi Pr. 31, 199004 St. Petersburg, Russia

A. V. Lyulin
Group Polymer Physics, Eindhoven Polymer Laboratories and Dutch Polymer Institute, Technische Universiteit Eindhoven, P.O. Box 513, 5600 MB Eindhoven, The Netherlands

(Received 29 June 2007; accepted 3 October 2007; published online 7 December 2007)

Brownian dynamics simulations with explicit hydrodynamic interactions have been employed to study generic effects of size and topology in noncovalent (Coulombic-driven) complexes formed by irregular-shaped hyperbranched polymers and linear polyelectrolytes. The behavior of the complexes was explored in detail in terms of static and dynamic properties, both in local and in the entire complex scale. The results were compared to previous studies on perfect dendrimers and other hyperbranched molecules where available. It was found that both molecular weight and structure may impart significant changes to key factors known to be associated with the ability of these systems to take part in relevant nanoscale applications. © *2007 American Institute of Physics*. [DOI: 10.1063/1.2802300]

I. INTRODUCTION

The driving force for the formation of complexes between oppositely charged linear polyelectrolytes (LPs) and hyperbranched polymers (HPs) in solution is mainly electrostatic attraction. Complex formation involving a polyelectrolyte and a macroion (e.g., between proteins and DNA or between colloidal particles and synthetic polyelectrolytes) is a usual phenomenon in living matter and plays a significant role in several novel nanoscale applications.[1] Recently, the ability of HPs to form complexes with DNA and other biological molecules has been experimentally and computationally explored,[2–4] and they were recognized as promising systems for targeted gene transfer.[3,5] Complexes formed by HP molecules and linear synthetic polyelectrolytes demonstrated their capacity to act as solubility enhancer, cytotoxicity reducer, and stabilizer against the enzymatic degradation agents for drug delivery purposes.[6]

Complexation process involving polyelectrolytes and macroions was found to depend on the chemical nature, the size, and the architecture of the participating molecules.[7,8] Features of candidate molecules for the formation of interpolyelectrolyte complexes, such as the possession of a high degree of functionality as well as versatility on the control of their chemical and structural characteristics are among the commonly desired attributes for such systems. Hyperbranched polymers appear as promising candidates[9] for complexation purposes due to their nanoscale dimensions, their high functionality, and the level of control recently developed in their synthetic strategies, which permit manipulation of their topological and chemical details.[10,11] Unlike the tedious multistep synthesis procedures followed for highly branched molecules bearing perfect dendritic structure, cost-effective single-step reactions can be applied for the nonregular-shaped hyperbranched polymers,[10] rendering them economically attractive alternatives to their regularly shaped counterparts for larger-scale production of complexed systems. In order to better understand their behavior and ultimately design systems with desired properties, a detailed description based on a molecular-level picture is necessary.

Computer simulations, being a technique which can afford a detailed control of structural and energetic parameters of the examined models, have proved a valuable tool for the investigation of systems bearing such complex architectures. In the study of Mulder *et al.*,[12] Brownian dynamics (BD) simulations have been performed for individual charged HPs of different topological structures, with terminal groups in the same generation and terminal groups distributed over all generations. Both types make their own demands to the method of synthesis. The molecular-weight and topology dependences of the HP size and radial mass distributions have been investigated.

The first Monte Carlo simulation of complexes formed by dendrimers with charged terminal groups and oppositely charged linear chains has been performed by Welch and Muthukumar.[13] Main attention has been paid to the statistical equilibrium properties of such complexes. The electrostatic interactions between charged groups were described by the screened Coulomb potential with the screening Debye radius determined by the salt concentration in the solution.

[a)]Author to whom correspondence should be addressed. Electronic mail: karatas@eng.auth.gr

Brownian dynamics computer simulations have been carried out by Lyulin *et al.*[14] of complexes formed by charged dendrimers and oppositely charged linear polymer chains of different degrees of polymerization. Bead-rod freely jointed models in the Debye-Hückel approximation without hydrodynamic interactions have been considered. It was concluded that the mean-square radius of gyration, the different monomer radial distribution functions, and the static structure factor for a dendrimer in a complex with long enough chains are very close to those for a single neutral dendrimer. The charged monomers of the linear chains were found to be located very close to the dendrimer terminal groups. For longer chains, the total number of the chain monomers adsorbed onto a dendrimer exceeded the number that is necessary for dendrimer neutralization, and the overcharging phenomenon was observed.

Theoretical description for the dynamics of dendritic molecules by Cai and Chen[15] considered the internal dynamics of trifunctional dendrimers built from beads (each having a friction constant ζ) and springs (each having an elasticity constant K) at θ conditions. In particular, they found that the normal modes can be categorized into two general groups: (i) normal modes involving bead motions with a mobile core and (ii) normal modes involving motions with an immobile core. The maximal relaxation time of the second group increases exponentially with the number of generations. It often represents the longest relaxation time $\tau_{\max}$ of the dendrimer as a whole; it was found that this longest relaxation time is proportional to the total number of beads, N, of the dendrimer, $\tau_{\max} \propto N$. For nonpenetrable dendrimer models with explicit hydrodynamic interactions present, Chen and Cai[16] calculated a slightly stronger dependence, $\tau_{\max} \propto N^{1.1}$, compared to the ideal dendrimer case.

In the present paper, BD simulations with explicit hydrodynamic interactions have been carried out for complexes of charged HPs of different molecular weights possessing extremely different topologies and oppositely charged LPs, thus preserving the total electroneutrality of the complexes. The main goal of the paper is to study generic effects of size, hyperbranched topology, and complexation on shape, monomer distributions, and segmental and global orientational dynamics of the complex constituents, and make, where possible, comparison with the same properties of individual objects and/or with previous relevant theoretical and computational studies. Results from the present study are expected to provide a guide for the specific attributes that could be appropriately engineered in order to create complexes with desired properties.

The rest of the paper is organized as follows. In Sec. II the model and the details of the simulation algorithm are presented. Section III A discusses static and conformational properties (such as monomer distributions, size, shape) of the simulated complexes. Local and global orientational motions as well as dynamics associated with size fluctuations of the complexes are described in Sec. III B. In Sec. IV the findings of the present work are summarized and relevant conclusions are drawn.

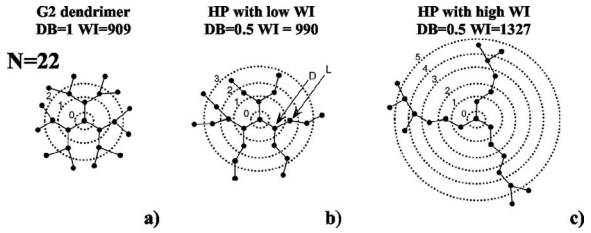

FIG. 1. Schematic representations of (a) a second generation perfectly branched dendrimer, (b) a randomly branched hyperbranched polymer with the same number of beads and DB=0.5, and (c) a HP with the same number of beads and DB but with different connectivity patterns described by WI. Characteristic dendritic and linear units of HP are indicated by arrows marked with D and L, respectively. Spatial limits of the generations of dendrimer and pseudogenerations of the HPs are indicated by the concentric circles.

II. MODEL AND SIMULATION ALGORITHM

Coarse-grained freely jointed bead-rod polymer systems, each one consisting of a single neutral HP or of a complex formed by a charged hyperbranched polymer and an oppositely charged LP, are generated. Monomers of HP and LP are represented as beads connected by rigid one-bond spacers of length l. Hyperbranched polymers with a trifunctional B_3 core (bead zero) and trifunctional AB_2 randomly branching groups are studied. Hence a $G=0$ HP consists of four beads including the core.[17] In the case of complexes, each bead of the hyperbranched polymer's terminal generation is set to carry a positive unit charge, while each bead of the linear polymer is set to carry a negative unit charge.

In general, hyperbranched structures are classified according to their number of monomer units, N, and degree of branching, DB, which is defined as[18]

$$\mathrm{DB} = \frac{2D}{2D+L}, \tag{1}$$

where D and L are the numbers of monomers with both its vicinal beads reacted (i.e., dendritic units) and with only one reacted vicinal bead (i.e., linear units), respectively. The so defined DB varies from 0 for a linear chain to 1 for a dendrimer or a fully branched HP. DB does not fully describe the connectivity, as it is obvious from the fact that both perfect dendrimers and less regular hyperbranched polymers can have a similar DB (Ref. 17) (e.g., Fig. 1). Therefore Wiener index (WI) is also employed to characterize the different structures.[19] WI is defined as the cumulative distance between all pairs of carbon atoms within the molecules measured in terms of the number of intervening bonds between two atoms. Herein it is calculated according to the following expression:[17]

$$\mathrm{WI} = \sum_{s=1}^{N-1} (V_{L,s} \times V_{R,s}), \tag{2}$$

where $V_{L,s}$ and $V_{R,s}$ are the number of beads in the left and that in the right, respectively, of the center of each bond, s. Hence N, DB, and WI describe unambiguously the branched structures of the present study.

In the present paper, the numbers of monomer units, N, used within each simulated hyperbranched structure are

TABLE I. Details of the simulated systems.

	Systems	HP (DB=0.5) WI	N	Generations	Pseudogenerations	N_T	LP N_L	Complex N_{tot}
1	G2 7 min	990	22	2	3	7	7	29
2	G2 7 max	1 327			5			
3	G3 13 min	6 384	46	3	5	13	13	59
4	G3 13 max	9 710			8			
5	G4 25 min	37 670	94	4	6	25	25	119
6	G4 25 max	60 351			11			
7	G5 49 min	210 726	190	5	8	49	49	239
8	G5 49 max	333 493			15			

equal to 22, 46, 94, or 190 (corresponding to generations 2, 3, 4, or 5 of perfect dendritic structure, respectively). The DB is chosen to be 0.5, a typical value for commercially available HPs, which stands between those of dendrimer and linear nonbranching structures.[20] The amounts of terminal beads, N_T, for the above mentioned molecules,

$$N_T = 2 + \mathrm{DB}\left(\frac{N}{2} - 1\right), \tag{3}$$

are 7, 13, 25, and 49 respectively.[12] In addition, for each of the above mentioned HP, structures representing two topological extremes are generated, one with a relatively low WI, describing a rather compact dendrimerlike structure (henceforth referred to as min), and one with a relatively high WI, describing a less compact, closer to a star-like shape (henceforth referred to as max). In general, structures with lower WI seem to develop their branches closer to their core, while structures with higher WI are branched toward the periphery (see Fig. 1).

In cases of complexes, a linear polyelectrolyte is added with the total number of oppositely charged beads, N_L, equal to the number of HP terminal beads, N_T, in order to preserve overall charge neutrality of the simulated systems.

Overall eight single HPs and eight complexes are simulated. Details about the systems examined can be found in Table I and Fig. 2.

As in the authors' previous works,[14,21,22] the Ermak-McCammon Brownian dynamics stochastic differential equation is integrated forward in time,[23]

$$\mathbf{r}_i = \mathbf{r}_\mathbf{i}^0 + \frac{\Delta t}{k_B T}\sum_j D_{\mathrm{ij}}^0 \cdot \mathbf{F}_j^0 + \mathbf{\Phi}_\mathbf{i}^0(\Delta t), \tag{4}$$

where $\mathbf{r}_i^0$ is the position vector for bead i before the Brownian dynamics time step, Δt, $k_B T$ is the Boltzmann factor, and $\mathbf{D}_{ij}^0$ is the diffusion hydrodynamic tensor. Hydrodynamic interactions are taken into account explicitly through the Rotne-Prager-Yamakawa tensor.[24] The strength of hydrodynamic interactions is set by the dimensionless hydrodynamic parameter h^*, which herein is chosen to be equal to 0.25 as in previous studies.[25] The main physicochemical interactions of beads are taken into account rigorously by means of appropriate potentials, giving a total force $\mathbf{F}_j^0$ [Eq. (5)], while as

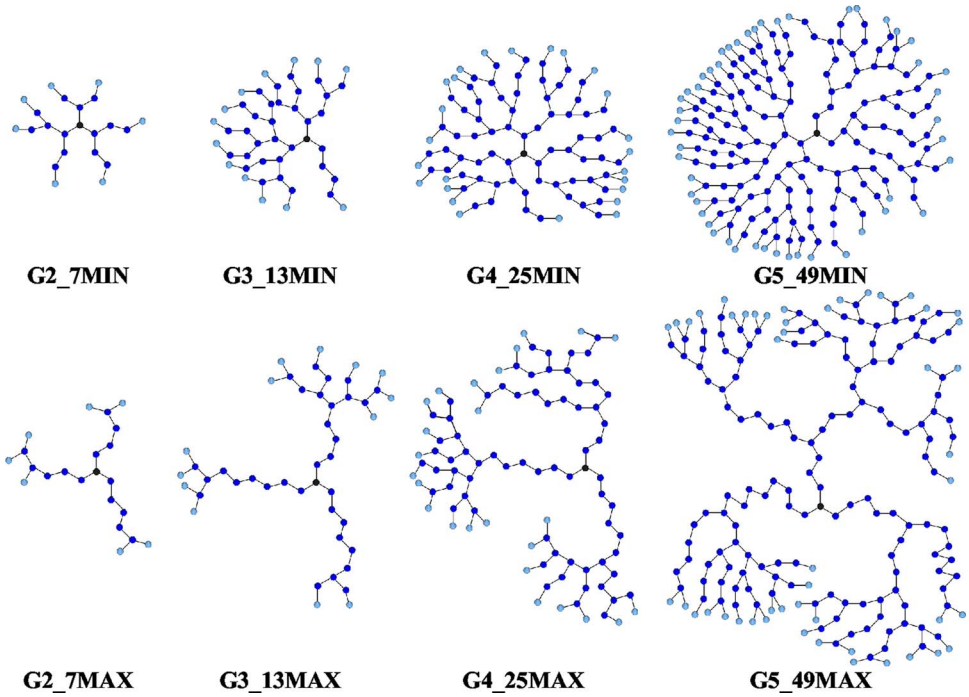

FIG. 2. (Color online) Schematic representations of two-dimensional projections of the studied HP models, which are simulated either as they are or in complex with linear polyelectrolytes. Charged (terminal) beads are shown in different colors.

usual in Brownian dynamics, the solvent is considered as a structureless viscous continuum with polymer-solvent collisions mimicked by a random force $\mathbf{\Phi}_i^0$.

$$\mathbf{F}_j^0 = \sum_k \mu_k \left(\frac{\partial \nu_k}{\partial \mathbf{r}_j} \right)_r^0 - \frac{\partial U_{\mathrm{LJ}}}{\partial \mathbf{r}_j^0} - \frac{\partial U_C}{\partial \mathbf{r}_j^0}. \tag{5}$$

In Eq. (5) ν_k is the equation of rigid constraint for the kth bond, μ_k is the corresponding Lagrange multiplier, U_{LJ} corresponds to Lennard-Jones potential for excluded-volume interactions and U_c corresponds to the Debye—Hückel potential for electrostatic interactions.

All the nonbonded beads in complex interact via a Lennard-Jones potential,

$$U_{\mathrm{LJ}}(r_{ij}) = 4\varepsilon_{\mathrm{LJ}} \left[\left(\frac{\sigma}{r_{ij}} \right)^{12} - \left(\frac{\sigma}{r_{ij}} \right)^{6} \right], \tag{6}$$

where r_{ij} is the distance between the ith and jth beads, $\varepsilon_{\mathrm{LJ}} = 0.3 k_B T$ and $\sigma = 0.8l$ are the characteristic energy and length parameters, and r_{cut} is the cutoff distance ($r_{\mathrm{cut}} = 2.5\sigma$). The attractive interactions between terminal beads in Eq. (6) are omitted.

Coulomb interactions of charged beads are taken into account through the Debye-Hückel potential:

$$\frac{U_C}{k_B T} = \lambda_B |q|^2 \sum_{i,j} \frac{\exp(-r_{ij}/r_D)}{r_{ij}}, \tag{7}$$

where r_{ij} is the distance between the ith and jth charged beads with charge equal to q (herein $|q| = 1$), λ_B is the Bjerrum length describing the strength of Coulomb interactions in a dielectric medium, and r_D is the Debye length which describes the screening of the electrostatic interactions due to the presence of counterions and salt in real solutions. Herein the Bjerrum length is considered to be equal to 1 and the Debye length is equal to 8.96l which corresponds to low aqueous salt concentration.[13]

The SHAKE algorithm with relative tolerance of 2×10^{-6} is used to maintain a fixed bond length.[26] Dimensionless quantities used in the simulations such as bond length l, thermal energy $k_B T$, translational friction coefficient ζ, and time $\zeta l^2 / k_B T$ are set to unity, while dimensionless integration step is chosen as $\Delta t = 10^{-4}$.

The initial configuration of each system is equilibrated for several runs of 2×10^6 time steps each, and then for each case seven more equal production runs are performed.

For more information about the simulation algorithm and initial configurations of the model, the reader can refer to the authors' previous works concerning dendritic polymers and complexes of dendrimers with linear chains.[12,14]

III. RESULTS AND DISCUSSION

A. Conformational properties

The effects of complexation, molecular size, and topology on the complexes' static/conformational properties were examined for all the complexes and compared to the behavior of the analogous noncomplexed neutral hyperbranched polymers. Geometric characteristics such as the size and shape of the systems were studied (i) by probing changes in the radius of gyration of the components,

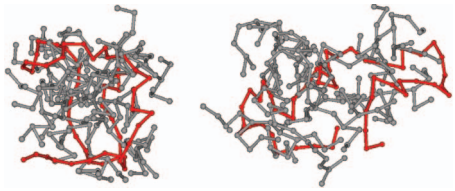

FIG. 3. (Color) Typical equilibrated structures for complexes of HPs with linear polyelectrolytes (LPs are shown in different colors) for the G5 min (left) and G5 max (right) models.

$$\langle R_g^2 \rangle = \frac{1}{N} \sum_{i=1}^{N} \langle (\mathbf{r}_i - \mathbf{r}_{\mathrm{c.m.}})^2 \rangle, \tag{8}$$

where N refers to the number of HP or linear polymer beads, while $\mathbf{r}_i$ and $\mathbf{r}_{\mathrm{c.m.}}$ denote the position vectors of the i_{th} bead and that of the center of mass, respectively, and (ii) by monitoring the degree of anisotropy via the behavior of the eigenvalues of the moment of inertia tensor of the HP molecules. The spatial arrangement of the hyperbranched and linear polymers' beads was examined by building histograms of the number of the beads as a function of their distance from the center of mass of the hyperbranched molecule [referred to as $n(r)$ henceforth], as well as by calculating the corresponding density profiles by dividing space in concentric spherical shells [referred to as $\rho(r)$]. Furthermore, relative arrangement of HP-linear bead pairs was inferred from the behavior of the respective radial distribution functions $g(r)$, calculated as

$$g(r) = \frac{1}{N} \left\langle \sum_{i=1}^{N} \sum_{j \neq 1}^{N} \delta(r - r_{ij}) \right\rangle, \tag{9}$$

where r_{ij} is the distance between a pair of beads. All analysis was performed at equilibrated structures as the ones shown in Fig. 3.

1. Radius of gyration

Figure 4 depicts the dependence of the root-mean-squared radius of gyration for the HP and the LP components of the examined complexes as a function of the corresponding number of monomers (beads).

The behavior of noncomplexed neutral HPs is depicted as well. Comparison between HPs bearing the two distinct architectures indicates that max WI models exhibit moderately larger (approximately by 25%) dimensions, which can be attributed to the more "open" structure characterizing HP molecules of this topology. Apart from a marginal difference between the size of the complexed and the single-neutral HPs of max WI topology, in general the size of charged HP molecules in the complexes is comparable to that of neutral HPs due to the charge neutralization induced by complexation with the linear polyelectrolytes. N dependence of the size of HPs of both the examined topologies, appears to follow closely the behavior of the single neutral HPs which to a good approximation is described by the scaling law $R_g \propto N^{1/3}$ that has also been reported for hyperbranched mol-

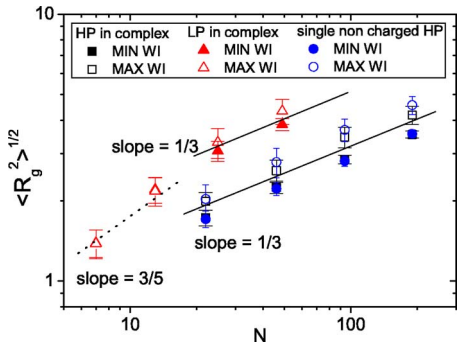

FIG. 4. (Color online) Collation of the dependences of radii of gyration for the linear and the HP molecules of the examined complexes as a function of the number of monomers. The behavior corresponding to neutral noncomplexed HP analogs is shown for comparison. Straight lines denote the scaling laws expected for perfect dendritic molecules (solid line) and for a linear chain with excluded volume interactions (dotted line).

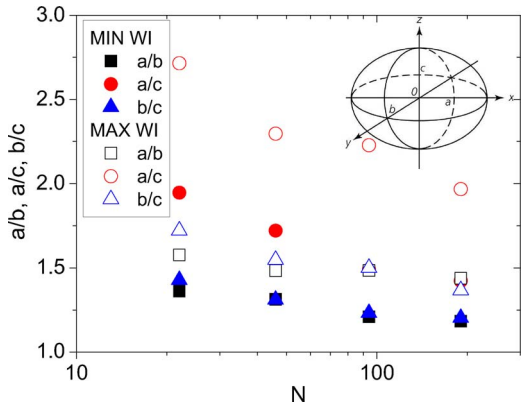

FIG. 5. (Color online) Dependence of the aspect ratios of the ellipsoid of inertia (shown in the schematic) on the total bead number of each complexed HP model.

ecules of perfect dendritic topology.[27,28] For the respective dependence of the dimensions of linear chains in complexes of both topologies, a single power law fit renders an exponent of ~0.55 with a correlation coefficient of 0.98. It seems however, that the data are better described by consideration of two scaling regimes: a low-N regime, where the radius of gyration scales to a good approximation with a power law commensurate to chains with excluded volume interactions (i.e., $R_g \propto N^{3/5}$), and a high-N regime where the size of the linear chains appears to follow that for the HP of the corresponding complex.

This observation implies that at small size complexes, the distributions of conformations of the linear chains are practically not affected by complexation. In contrast, at large size complexes due to the larger number of Coulombic pairs between LP monomers and charged HP beads, the distribution of LP conformations is strongly affected by the HP behavior.

2. Shape anisotropy

To further elaborate on the effects of topology and size to the geometrical anisotropy of the examined models, we have resorted to the calculation of the dimensions of the ellipsoid of inertia for each complexed system. The lengths of the semiaxes of the ellipsoid a, b, and c, can be calculated according to

$$a = \sqrt{\frac{5}{2m}(I_x + I_y - I_z)}, \quad b = \sqrt{\frac{5}{2m}(I_x + I_z - I_y)},$$

$$c = \sqrt{\frac{5}{2m}(I_y + I_z - I_x)},$$

where $I_x > I_y > I_z$ represent the eigenvalues of the moment of inertia tensor and m denotes the total mass of the examined system. The results are described in Fig. 5 for both of the complexed systems, where the aspect ratios are plotted as a function of the number of monomers.

A general observation which applies to all the studied models is the decrease of anisotropy upon increasing of the HP size in analogy to what was observed for perfect dendrimers.[27] It is worth noticing though that models corresponding to the max WI assume a markedly higher anisotropy compared to the min WI systems. This notion holds true when comparison is made between the noncomplexed neutral HPs of the two topologies as well. This difference is particularly enhanced as far as it concerns the longer semiaxis, indicating a much larger degree of elongation of the less compact systems. It should also be mentioned that neutral single HP systems of the max WI topology (not shown here) exhibit an even more elongated shape (by about 10%) compared to their complexed analogs. Actually this is the origin for the somewhat higher radius of gyration of the single max WI systems which was noted in Fig. 4.

3. Bead distributions and density profiles

Figure 6 depicts the bead distribution profiles of the HP molecules and the linear chains in complexes with respect to the HP center of mass, grouped according to the topology of the models. For both the examined architectures, HP and LP profiles overlap, indicating on average a full interpenetration of LP chains within the HP structure. Due to the less compact conformations assumed by the max WI systems, their distributions are significantly broader compared to their min WI analogs. This trend is followed by the bead profiles of the linear chains in the corresponding complexes as well. Distributions of the LP chains are essentially determined from those of the charged HP beads which follow the same pattern described for the overall HP bead profiles.

The profiles of HPs in complexes and those of single neutral HPs practically coincide for min WI systems. For max WI models, while in the smaller generation system G2,

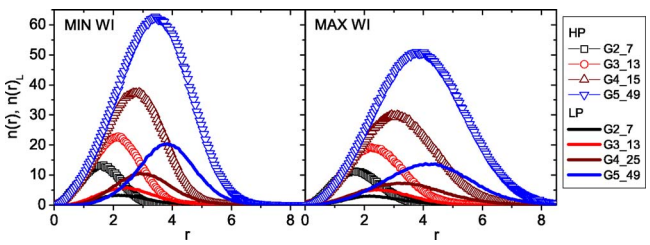

FIG. 6. (Color online) Bead number profiles of the HP, $n(r)$, and LP, $n(r)_L$, molecules in complexes for the min WI (left) and the max WI (right) systems.

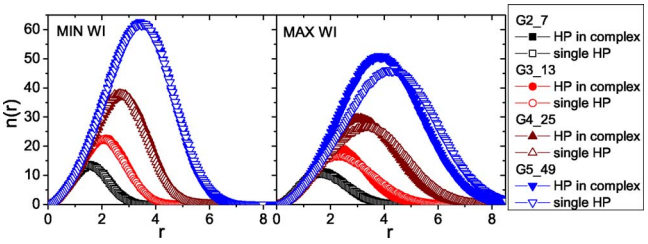

FIG. 7. (Color online) Comparison of bead distribution functions for min (left) and max (right) WI systems with their single noncharged analog.

a similar degree of overlap is observed between the profiles of complexed and noncomplexed neutral HPs, deviations start emerging at larger size systems, with those of the complexed systems being less widespread as shown in Fig. 7.

This observation is consistent with the moderately lower degree of elongation (i.e., the possibility to span smaller distances) of the complexed max WI systems compared to their neutral noncomplexed analogs as discussed earlier.

These similarities/differences are expectedly reflected in the corresponding density profiles in systems of the two examined topologies. Figure 8 displays the density profiles $\rho(r)=n(r)/V(r)$ where $V(r)$ represents the volume of a spherical shell at distances between r and $r+dr$ from the center of mass of the HP.

A characteristic feature of the profiles describing min WI models is a prominent maximum at a distance close to the bond length. This can be ascribed to the higher branching density assumed by these systems, which renders the region close to the topological center less accessible to other beads. This behavior is consistent with the previously described bead number distributions (see Fig. 6), where it can be discerned that LP bead profiles in complexes with min WI HPs are practically zero at distances below a bond length. In contrast, density profiles of max WI HPs appear more homogeneous, in line with the more open interior of this topology.

The coincidence observed in bead distributions of min WI models between the complexed and single neutral HPs is naturally observed between the corresponding density profiles (not shown here) as well. Similarly, the differences noticed in the distributions between complexed and single HPs of max WI topology are also reflected in their density profiles. As the size of the models grows, the profiles of the

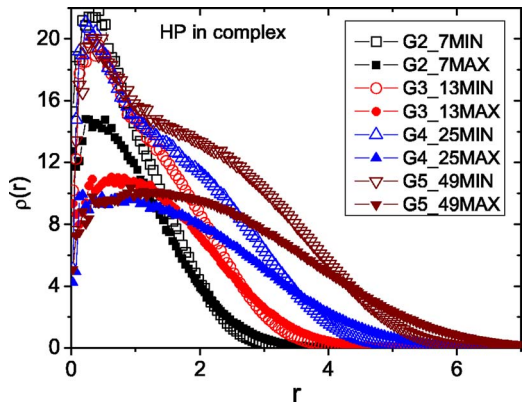

FIG. 8. (Color online) Density profiles of the HP molecules in complexes.

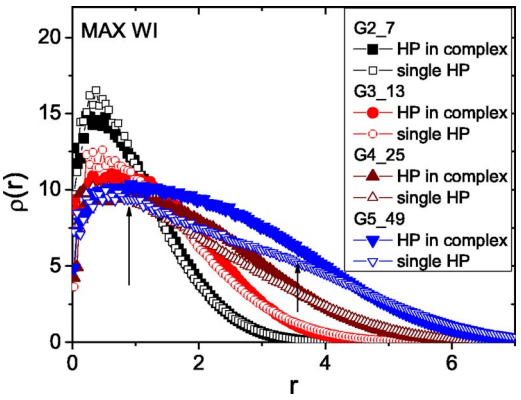

FIG. 9. (Color online) Comparison between the density profiles of systems bearing the max WI structure in complexes and in noncomplexed neutral states. Arrows denote the development of a bimodal character in the larger single noncharged HP profile.

complexed systems assume a more homogeneous character, while at the single HP models, there are indications for the development of a bimodal profile at the larger system examined (Fig. 9). To justify such behavior, one must resort to the topological details of the max WI G5 model (see Fig. 2). As shown, this structure is featured by the existence of individual dendrons with a strong local density contrast (in terms of bead population) with that of the interior, which can rationalize the appearance of such bimodal density profile. The amplitude of the second shoulder near $r\sim 3.5$ is expected to be more pronounced to the G5 model than to its G4 analog due to the higher number of peripheral dendrons characterizing the larger system.

On the other hand, the presence of linear polymer in the complexes works against the development of density inhomogeneities. Indeed, since LP explores the entire HP interior (see the bead distributions in Fig. 6), it enhances the backfolding effect of the terminal HP beads due to their Coulomb attraction to the linear chain's beads, thus promoting homogenization of the HP density distribution.

4. Spatial arrangement of HP-linear bead pairs

Figure 10 displays the cross-pair radial distributions functions between HP and LP beads for all the examined models. While no difference is shown between distributions of systems possessing different topologies but the same molecular weight (see also the expanded view in the inset), a systematic broadening toward larger distances is observed when moving from smaller to larger system sizes.

In addition, a characteristic feature of all the distributions is the existence of two peaks at distances moderately higher than σ and 2σ, respectively. The peak at the smaller separation is expected due to the close contacts between charged LP and HP beads, while the maxima at the larger distance are a direct effect of the bead connectivity of the linear chain (i.e., a HP bead that is at a distance close to σ with a LP bead, it is also a neighbor of a LP bead connected to the latter). The broadening of the distributions observed in the larger size models should be attributed to the wider range of possible HP-LP bead distances due to increased population of the HP-LP pairs and the larger range of spatial dimen-

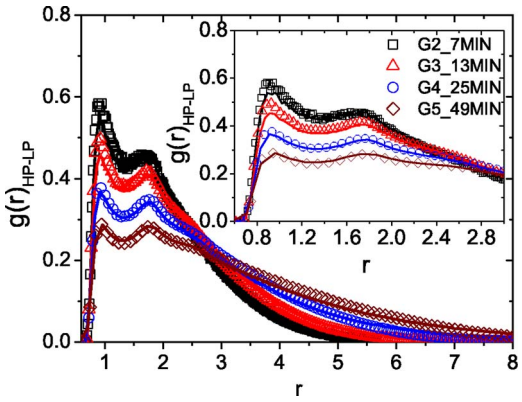

FIG. 10. (Color online) Cross-pair radial distribution functions concerning all the HP and LP beads. Symbols represent min WI systems, while lines passing through the points denote the corresponding max WI distributions. The inset is an expanded view of the main panel at a smaller window of distances.

sions spanned by the two components of the complexes. The above assignment of the peaks' identities is corroborated by the behavior of the analogous cross-pair distributions between charged beads only, as illustrated in Fig. 11.

Evidently, the amplitude (height) of the short-distance peak is augmented compared to the one observed in the all-bead distributions, since Coulomb attractions increase the probability of finding close contacts between charged-bead pairs. On the other hand, the second peak loses amplitude, since all pairs between the noncharged HP beads and the LP beads do not contribute any more.

B. Dynamic properties

1. Local segmental orientational mobility

Local and global dynamic orientational processes referring to each complex constituent separately are studied in terms of time autocorrelation functions (ACFs). Analysis of all the ACFs was performed by means of the calculation of the distribution of (exponential) relaxation times (DRTs),[29], through which a correlation function $C(t)$ is described as a continuous superposition of single exponential processes,

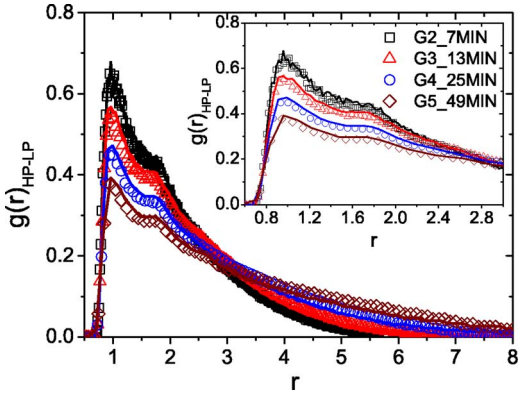

FIG. 11. (Color online) Cross-pair radial distribution functions between charged HP and LP beads. Symbols represent min WI systems, while lines passing through the points denote the corresponding max WI distributions. The inset is an expanded view of the main panel at a shorter range of distances.

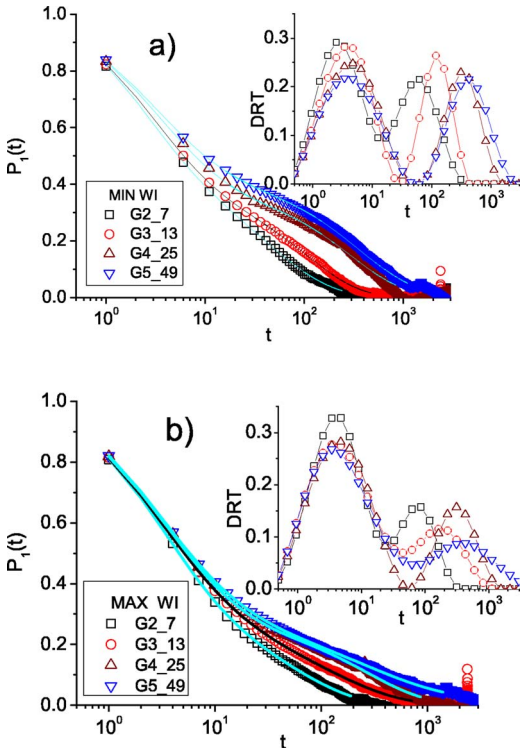

FIG. 12. (Color online) P_1 ACFs for a HP bond unit vector for G2–G5 complexes with (a) min WI and (b) max WI. Solid lines through the points represent the fits resulting from the DRT analysis. Insets: corresponding distribution functions of relaxation times.

without any *a priori* assumption regarding its functional form, according to

$$C(t) = \int_{-\infty}^{\infty} F(\ln(\tau)) e^{-t/\tau} d \ln \tau. \tag{10}$$

In this expression $F(\ln(\tau))$ represents the calculated normalized distribution function. Distinct peaks appearing in the distribution correspond to dynamic processes well separated in time scale. A characteristic time for each process can be estimated through the first moment of the calculated distribution,

$$\langle \tau \rangle = \frac{\int_{\tau_i}^{\tau_f} F(\ln(\tau)) \tau d \ln \tau}{\int_{\tau_i}^{\tau_f} F(\ln(\tau)) d \ln \tau}, \tag{11}$$

where τ_i and τ_f denote the time limits within which each peak extends. In the case of symmetric peaks, a good approximation for the characteristic time can be provided by the time location of the peak. An overall average (i.e., including all the processes) can be calculated when the integration range covers the entire time window.

The first order Legendre polynomial ACF $P_1(t)$,

$$P_1(t) = \frac{1}{N} \sum_i \langle \mathbf{u}_i(0) \mathbf{u}_i(t) \rangle, \tag{12}$$

has been evaluated for all the bond unit vectors **u** for HP or linear chain in simulated complexes of different sizes and topologies. The relaxation of these ACFs is clearly nonexponential as illustrated in Fig. 12 (only ACFs for HP in complexes are shown; a qualitatively similar picture is valid for

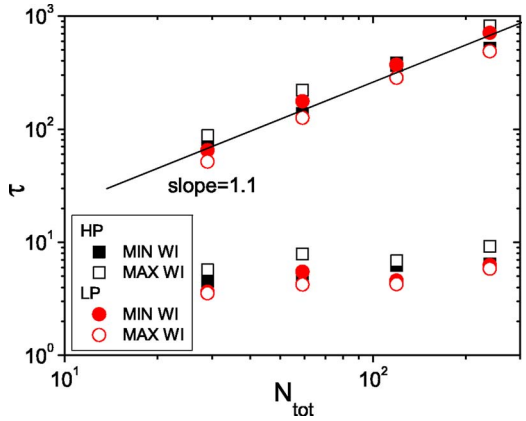

FIG. 13. (Color online) Relaxation times of the fast and slow processes for P_1 ACFs for HPs and LPs in complexes of different sizes and topologies. Error bars are of the order of the symbols' size. Line denotes the scaling law $\tau \propto N^{1.1}$.

linear-chain ACFs). A rather pronounced shoulder at $t > 100$ appears especially for HPs with minimal Wiener index, indicating the onset of a slow relaxation process. This slow relaxation process has strong molecular-weight dependence, since it is shifted to larger times (see the corresponding peak locations) upon increasing of the size of the model.

Indeed the detailed examination of the orientational dynamics by DRT analysis prompts the existence of two independent relaxational processes, with strikingly different molecular-weight dependences (see insets in Fig. 12).

At short times, $t \sim 5$, for complexes of both topologies, there is a relaxation process which does not depend on the molecular weight and which is consistent with the fast tumbling motion of individual bonds. Its magnitude is approximately the same for complexes with different WIs. The position of the slower process at $t > 100$ is clearly shifted to larger times with increasing molecular weight. The amplitude of this slow segmental relaxation process appears higher in systems with min WI. The higher intensity of the slow relaxation process for min WI HPs can be understood by the fact that due to the dense connectivity pattern characterizing this topology (see also the corresponding density profiles in Fig. 8), a larger percentage of bonds relaxes via the overall rotation of the HP compared to the max WI HPs; in max WI, HP bond reorientation within the more abundant nonbranched parts is less hindered, and thus overall HP rotation is less important for their relaxation.

For linear chains in complexes, the relaxation of the corresponding P_1 ACFs (not shown here) is also characterized by two processes, with and without a pronounced molecular-weight dependence. The characteristic relaxation times corresponding to these processes (calculated as first moments of the corresponding DRTs) are plotted as functions of molecular weight of the whole complex (which is mainly determined by the mass of the HP polymer) in Fig. 13 for both HPs and linear chains in all the examined complexes.

Corresponding relaxation times for the fast process are about 5–6 and are the same within the statistical error for all simulated HPs and linear polymers and do not depend on the specific topology of the objects. The relaxation times of the

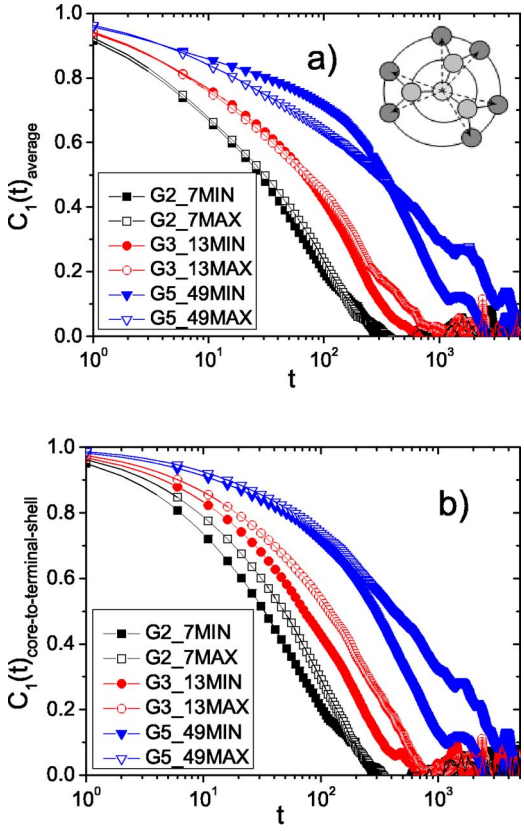

FIG. 14. (Color online) (a) Time dependence for the overall average core to g shell unit vector ACFs for HPs of different sizes and topologies. The schematic illustrates the definition of the core to g shell vectors. (b) analogous core to terminal shell ACFs for the examined HP models. G4 models are omitted from both pictures for clarity of presentation.

slow relaxation process for the HPs in complexes of different topologies and linear chains are close to each other.

The molecular-weight dependence of the slow relaxational process indicates the influence of the overall rotation of the complex (which becomes slower upon increasing the molecular weight) on the orientational motion of individual bonds. This molecular-weight dependence of the relaxation times for the slowest process can be described by a power law, $t \propto N^{\alpha}$ with $\alpha \approx 1.1$. This scaling law will be discussed further below in conjunction with the time scales of the ACFs for global rotation.

2. Global orientational motion

To investigate the orientational dynamics on much larger spatial scales, the first order Legendre polynomials ACFs $C_1(t)$ are calculated for overall average core to g shell and core to terminal shell [Fig. 14(a) and 14(b)] unit vectors $\mathbf{g}$ [see inset schematic in Fig. 14(a)],

$$C_1(t) = \langle \mathbf{g}(0)\mathbf{g}(t) \rangle. \tag{13}$$

At the entire complex scale, appreciable differences in the average rotational relaxation times for complexes of different topologies are only observed at the larger size systems: rotational relaxation times for large HPs with min WI are slightly smaller compared to large HPs with max WI. This finding might be associated with the more open structure of the max WI topology, particularly for the G5 system,

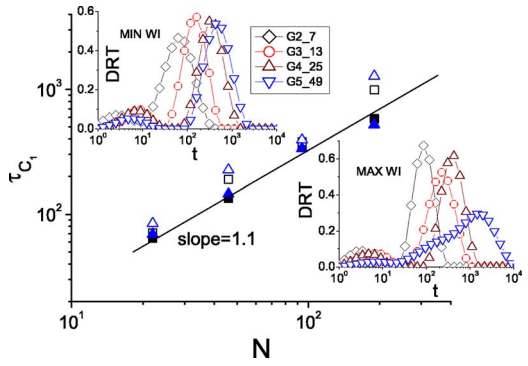

FIG. 15. (Color online) Average relaxation times of the correlation functions shown in Fig. 14. Overall core to g shell average [max (□) and min (■)] and core to terminal shell average [max (△) and min (▲)]. Error margins are within the size of the symbols. Line denotes the theoretical scaling law as described in the text. Insets: distributions of relaxation times (DRTs) for core to terminal ACFs. Symbols are common in both insets.

which assumes the most elongated conformations (see Fig. 5). However, orientational motion at the peripheral (terminal) shells appears systematically faster (i.e., correlation functions relax at earlier times) for HPs with min WI as shown in Fig. 14(b).

This is likely due to much stronger hydrodynamic interactions between particles of compact structures with min WI. For more sparse HPs with max WI, the hydrodynamic interactions between different segments are less important, the free-draining limit of the dynamics should be considered, and the corresponding orientational relaxation times should be larger.

This effect is probably also responsible for the slightly smaller relaxation times of the slow process for HPs in complexes with min WI plotted in Fig. 13 earlier for the local orientational motions of individual bonds and again is an indication of the influence of the overall rotation in the local bond dynamics.

The DRT analysis of the C_1 ACFs (insets in Fig. 15) indicates one principal relaxational process with strong molecular-weight dependence, reflecting the global rotation of the HP in a complex. The molecular-weight dependence of the characteristic relaxation times (main panel in Fig. 15), which seems to describe the behavior of the majority of the models, is consistent with a theoretically predicted $t \propto N^{1.1}$ scaling for the maximal relaxation time in neutral dendrimer models with inclusion of hydrodynamic interactions[16] and is similar to the one observed for the slow process in the relaxation of the P_1 ACFs for individual bonds discussed earlier. Particularly for the max WI G5 models, we should also note their broader or perhaps bimodal DRT spectra (see inset for max WI models in Fig. 15) which might be interpreted as an indication of the existence of an additional dynamic process. Such intermediate-scale processes were observed in large generation neutral dendrimers[27] and were attributed to the development of a strong dynamic contrast within the dendritic structure as the dendrimer sizes grow.

For small generation hyperbranched polymers, however, one can conclude that the theoretically predicted scaling is probably universal and does not depend much on the topology of the branched system. The charges of course should

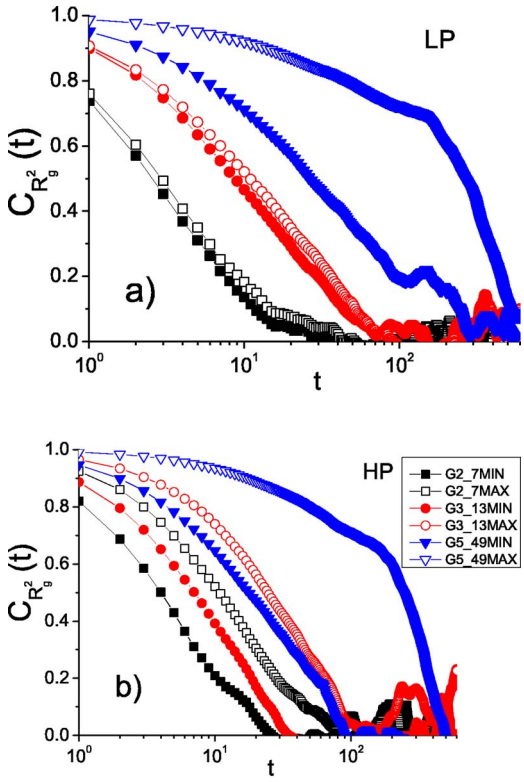

FIG. 16. (Color online) Time dependence of ACFs for square radius of gyration for (a) LPs and (b) HPs in complexes of different sizes and topologies [the symbols correspond to the same complexes in (a) and (b)]. G4 systems are omitted for clarity of presentation.

modify this scaling law, but the presence of the oppositely charged linear chain in a complex makes the global HP dynamics more "neutrallike."

3. Size fluctuations

The dynamics of size fluctuations are studied through the autocorrelation functions $C_{R_g^2}(t)$ for the square radius of gyration,

$$C_{R_g^2(t)} = \frac{\langle R_g^2(0) R_g^2(t) \rangle - \langle R_g^2 \rangle^2}{\langle R_g^4 \rangle - \langle R_g^2 \rangle^2}, \tag{14}$$

where R_g is the radius of gyration for HP or linear chain in a complex as shown in Fig. 16.

A common observation in both HP and LP behaviors is a clear molecular-weight dependence, i.e., the size relaxation becomes slower for larger size objects. Moreover, there is a systematic difference in the relaxation of this function for complexes of different topologies. It always appears slower (i.e., decorrelation is attained at longer time scales) in complexes formed by (larger in size) HPs with maximal WI. This difference is more prominent in the HP constituents of the complexes. The average relaxation times corresponding to the $C_{R_g^2}(t)$ ACFs of HP in complexes are shown in Fig. 17 together with the times extracted from their noncomplexed neutral analog (corresponding ACFs not shown here).

A visual comparison with Fig. 15 shows that times describing size fluctuations are always faster compared to those required for global rotation of HPs in complexes, in consensus with the behavior observed in Brownian[21] and molecular

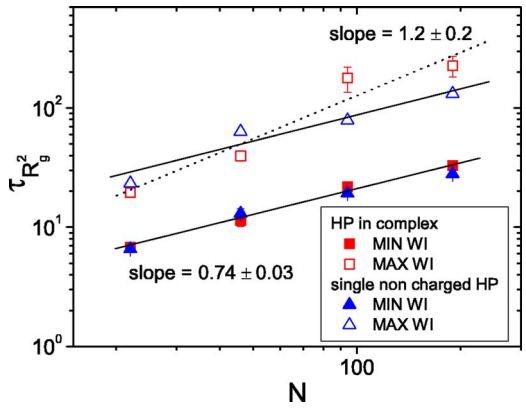

FIG. 17. (Color online) Average relaxation times of $C_{R_g^2}$ ACFs for single neutral HP models (▲,△) and for HPs in complexes (■,□). Lines through the points (solid for min WI and dotted for complexed max WI models) represent best fits for HPs in complexes. The solid line through points corresponding to single max WI models has the same slope as the one calculated for the min WI models.

dynamics[30] simulations for neutral dendrimers. The coincidence between times for global reorientation and size fluctuations predicted theoretically for perfect dendrimer models was attributed to the utilization of a linearized version of the Langevin equation; it was surmised that in real systems, size fluctuations should be realized in shorter time scales[16] since the latter depend mostly on internal motions which are in principle faster than global reorientation. The molecular-weight dependence of the average times describing size fluctuations was found to scale with an exponent lower than unity for min WI HPs, both for complexed and noncomplexed neutral models as illustrated in Fig. 17, in line with previous studies in neutral dendrimer systems.[21] For max WI systems of the complexed HPs, however, an optimal linear fit in logarithmic axes furnishes a larger exponent, indicating that for this topology, complexation influences appreciably the internal relaxation modes of the hyperbranched molecule.

IV. SUMMARY/CONCLUSIONS

In this work we have examined the effects of molecular weight, topology, and complexation in the static and dynamic behavior of terminally charged hyperbranched models bearing an imperfect dendritic structure, which form complexes with linear oppositely charged neutralizing chains. It was found that each of these three factors may affect in a distinct manner the properties of the resulting complexes.

In terms of static characteristics, the molecular-weight dependence of the average size (as expressed by the radius of gyration) of the HP in complexes was found to follow the $R_g \propto N^{1/3}$ law indicating three-dimensional space-filling objects as was noted in previous studies of regular dendrimers. Complexation resulted to a moderate decrease in average size only for the max WI HP models compared to their dimensions in a noncomplexed neutral state. In the complexed state and at constant molecular weight, max WI systems exhibited larger average dimensions from their min WI analog by approximately 25%, while they also assumed more elongated shapes. Overall, for both topologies, shape anisotropy decreases upon increase of molecular weight, in line with past findings concerning perfect dendrimers. In terms of local bead and density profiles, max WI systems always displayed broader distributions compared to the same molecular weight min WI HPs. While min WI HPs were found to behave closely to their noncomplexed analogs, complexation in max WI models resulted to somewhat narrower bead profiles while promoting homogenization of their density distributions. Average bead distances were not sensitive to topological details but depended on molecular weight (the higher the molecular weight, the broader the range of possible distances between bead pairs).

In terms of dynamic properties, in local length scales, two characteristic dynamic processes were identified: (i) one with a molecular weight and topology independent time scale and amplitude, associated with a very fast bond tumbling motion, and (ii) a slower mode which exhibits a topology insensitive but molecular-weight-dependent time scale and topology-dependent amplitude. This process is closely related to the overall HP rotation in the complex. Its topology-dependent amplitude arises from the distinctly different branching patterns characterizing the two extreme architectures. A similar picture describes local dynamics of the linear polymer as well, indicating the high impact of complexation to the dynamics of the "bound" chain. At the length scale of the entire HP, with a possible exception of the large size max WI models, the average time scale of the rotational motion seems to follow the molecular-weight dependence predicted for perfect dendritic molecules with hydrodynamic interactions present. The topological differences result to moderately faster dynamics for the more compact min WI structures. The characteristic time for size fluctuations appears at all cases faster than the overall rotational motion as was documented in earlier studies for regular dendrimers. Effects of the architecture are manifested through the faster dynamics for this kind of motion assumed by max WI systems and by the different molecular-weight dependences of the corresponding time scale exhibited by the two topological extremes.

In general, compared to the behavior of HPs of regular dendritic structure, it was found that in several aspects, nonregular hyperbranched molecules participating in such complexes behave similarly to their perfect dendrimer analogs constituting thus a cheaper alternative when complexed systems are required. Moreover, they offer the possibility of controlling properties such as geometry, size, local density, and time scale for size fluctuations and for relaxation in local and global scales. It is therefore believed that such systems can be promising cost-effective candidates in applications where control of the above mentioned attributes is a crucial parameter for accomplishment of the desired results (e.g., gene transfer and targeted drug delivery).

ACKNOWLEDGMENTS

This work is financially supported by the Hellenic General Secretariat for Research and Technology under the framework of the PENED 2003 program (Grant No. 03E△716). S.V.L. acknowledges funding from NWO Grant No. 047.019.001 and RFBR Grant No. 05-03-32450.

[1] S. Ulrich, M. Seijo, and S. Stoll, Curr. Opin. Colloid Interface Sci. **11**, 268 (2006).
[2] D. Leisner and T. Imae, J. Phys. Chem. B **108**, 1798 (2004).
[3] C. S. Braun, J. A. Vetro, D. A. Tomalia, G. S. Koe, J. G. Koe, and C. R. Middaugh, J. Pharm. Sci. **94**, 423 (2005).
[4] P. K. Maiti and B. Bagchi, Nano Lett. **6**, 2478 (2006).
[5] D. S. Shah, T. Sakthivel, I. Toth, A. T. Florence, and A. F. Wilderspin, Int. J. Pharm. **208**, 41 (2000).
[6] E. Chiellini, *Biomedical Polymers and Polymer Therapeutics* (Kluwer Academic, New York, 2002); D. K. Smith, A. R. Hirst, C. S. Love, J. G. Hardy, S. V. Brignell, and B. Huang, Prog. Polym. Sci. **30**, 220 (2005).
[7] T. Imae and A. Miura, J. Phys. Chem. B **107**, 8088 (2003).
[8] S. Holappa, L. Kantonen, T. Andersson, F. Winnik, and H. Tenhu, Langmuir **21**, 11431 (2005); E. M. Mateescu, C. Jeppesen, and P. Pincus, Europhys. Lett. **46**, 493 (1999).
[9] C. Gao and D. Yan, Prog. Polym. Sci. **29**, 183 (2004).
[10] C. R. Yates and W. Hayes, Eur. Polym. J. **40**, 1257 (2004).
[11] U. Boas, J. B. Christensen, and P. M. H. Heegaard, J. Mater. Chem. **16**, 3786 (2006); M. G. McKee, S. Unal, G. L. Wilkes, and T. E. Long, Prog. Polym. Sci. **30**, 507 (2005).
[12] T. Mulder, A. V. Lyulin, P. van der Schoot, and M. A. J. Michels, Macromolecules **38**, 996 (2005).
[13] P. Welch and M. Muthukumar, Macromolecules **33**, 6159 (2000).
[14] S. V. Lyulin, A. A. Darinskii, and A. V. Lyulin, Macromolecules **38**, 3990 (2005).
[15] C. Z. Cai and Z. U. Chen, Macromolecules **30**, 5104 (1997).
[16] Z. Y. Chen and C. Z. Cai, Macromolecules **32**, 5423 (1999).
[17] A. H. Widmann and G. R. Davies, Comput. Theor. Polym. Sci. **8**, 191 (1998).
[18] D. Holter, A. Burgath, and H. Frey, Acta Polym. **48**, 30 (1997).
[19] H. Wiener, J. Am. Chem. Soc. **69**, 17 (1947).
[20] X. S. Feng, D. Taton, E. L. Chaikof, and Y. Gnanou, J. Am. Chem. Soc. **127**, 10956 (2005).
[21] S. V. Lyulin, A. A. Darinskii, A. V. Lyulin, and M. A. J. Michels, Macromolecules **37**, 4676 (2004).
[22] S. V. Lyulin, A. V. Lyulin, A. A. Darinskii, and I. Emri, Polym. Sci., Ser. A Ser. B **47**, 1217 (2005).
[23] D. L. Ermak and J. A. McCammon, J. Chem. Phys. **69**, 1352 (1978).
[24] J. Rotne and S. Prager, J. Chem. Phys. **50**, 4831 (1969); H. Yamakawa, *ibid.* **53**, 436 (1970).
[25] A. V. Lyulin, D. B. Adolf, and G. R. Davies, Macromolecules **34**, 3783 (2001); S. V. Lyulin, A. V. Lyulin, and A. A. Darinskii, Polym. Sci., Ser. A Ser. B **46**, 196 (2004).
[26] J. P. Ryckaert and A. Bellemans, Chem. Phys. Lett. **30**, 123 (1975).
[27] K. Karatasos, D. B. Adolf, and G. R. Davies, J. Chem. Phys. **115**, 5310 (2001).
[28] S. V. Lyulin, A. V. Lyulin, and A. A. Darinskii, Polym. Sci., Ser. A Ser. B **46**, 189 (2004).
[29] S. Provencher, Comput. Phys. Commun. **27**, 229 (1982).
[30] M. Murat and G. S. Grest, Macromolecules **29**, 1278 (1996).